



RESEARCH ARTICLE

10.1002/2016JF003842

Key Points:

- A subglacial hydrology model produces a multiyear simulation of water pressure coherent with observed surface uplift
- The model results confirm the existence of two distinct modes of behavior of the subglacial water pressure in Russell region

Supporting Information:

- Movie S1
- Supporting Information S1

Correspondence to:

B. de Fleurian,
basile.defleurian@uib.no

Citation:

de Fleurian, B., M. Morlighem, H. Seroussi, E. Rignot, M. R. van de Broecke, P. K. Munneke, J. Mouginot, P. C. J. P. Smeets, and A. J. Tedstone (2016), A modeling study of the effect of runoff variability on the effective pressure beneath Russell Glacier, West Greenland, *J. Geophys. Res. Earth Surf.*, 121, doi:10.1002/2016JF003842.

Received 3 FEB 2016

Accepted 22 SEP 2016

Accepted article online 29 SEP 2016

©2016. The Authors.

This is an open access article under the terms of the Creative Commons Attribution-NonCommercial-NoDerivs License, which permits use and distribution in any medium, provided the original work is properly cited, the use is non-commercial and no modifications or adaptations are made.

A modeling study of the effect of runoff variability on the effective pressure beneath Russell Glacier, West Greenland

Basile de Fleurian¹, Mathieu Morlighem¹, Helene Seroussi², Eric Rignot^{1,2}, Michiel R. van den Broeke³, Peter Kuipers Munneke³, Jeremie Mouginot¹, Paul C. J. P. Smeets³, and Andrew J. Tedstone⁴

¹Department of Earth System Science, University of California Irvine, Irvine, California, USA, ²Jet Propulsion Laboratory, California Institute of Technology, Pasadena, California, USA, ³Institute for Marine and Atmospheric Research, Utrecht University, Utrecht, Netherlands, ⁴School of Geosciences, University of Edinburgh, Edinburgh, UK

Abstract Basal sliding is a main control on glacier flow primarily driven by water pressure at the glacier base. The ongoing increase in surface melting of the Greenland Ice Sheet warrants an examination of its impact on basal water pressure and in turn on basal sliding. Here we examine the case of Russell Glacier, in West Greenland, where an extensive set of observations has been collected. These observations suggest that the recent increase in melt has had an equivocal impact on the annual velocity, with stable flow on the lower part of the drainage basin but accelerated flow above the Equilibrium Line Altitude (ELA). These distinct behaviors have been attributed to different evolutions of the subglacial draining system during and after the melt season. Here we use a high-resolution subglacial hydrological model forced by reconstructed surface runoff for the period 2008 to 2012 to investigate the cause of these distinct behaviors. We find that the increase in meltwater production at low elevation yields a more efficient drainage system compatible with the observed stagnation of the mean annual flow below the ELA. At higher elevation, the model indicates that the drainage system is mostly inefficient and is therefore strongly sensitive to an increase in meltwater availability, which is consistent with the observed increase in ice velocity.

1. Introduction

Ice surface velocity is the result of both internal deformation of the ice body and basal slip defined as the combination of glacier sliding on bedrock and, if present, the deformation of a sediment layer between the glacier and bedrock [Cuffey and Paterson, 2010]. Basal slip has been measured on a number of mountain glaciers to determine that this component accounts for about half of the observed surface displacement [Cuffey and Paterson, 2010], but it can also account as much as 95% of the overall surface velocity in some cases [e.g., surging glaciers Kamb *et al.*, 1985]. Observations on ice sheets are more scarce, but the available data suggest that basal slip plays a major role in the observed surface velocity of fast-flow regions of the ice sheets [e.g., Morlighem *et al.*, 2013; Luthi *et al.*, 2002; Engelhardt and Kamb, 1998].

Contrary to internal deformation, which is well known and constant in time in the absence of major glacier thinning, basal slip varies seasonally and interannually [e.g., Hewitt and Fowler, 2008]. It is commonly agreed that water pressure at the glacier base is the main driver for fluctuations in basal velocity of land-terminating glaciers [e.g., Iken *et al.*, 1993], but a simple relationship between runoff volume and basal water pressure does not exist and the modeling of subglacial hydrology remains an open question [Flowers, 2176]. Moreover, the difficulty of accessing the glacier base makes it challenging to obtain observations required to evaluate theories of basal slip.

On Russell Glacier, observations show that large changes in meltwater availability (e.g., in year 2012 runoff was twice as large as in year 2009) seem to lead to a stagnation or even a slowdown in annual ice velocity at low elevation (below the Equilibrium Line Altitude, ELA) [Sundal *et al.*, 2011; Sole *et al.*, 2013; Tedstone *et al.*, 2013; van de Wal *et al.*, 2015]. The seasonal variability shows an acceleration at the onset of the melt season, linked to the availability of surface meltwater, while the subglacial drainage system is still weakly developed [e.g., Bartholomew *et al.*, 2010; Palmer *et al.*, 2011], which is followed by a significant slowdown when the volume of

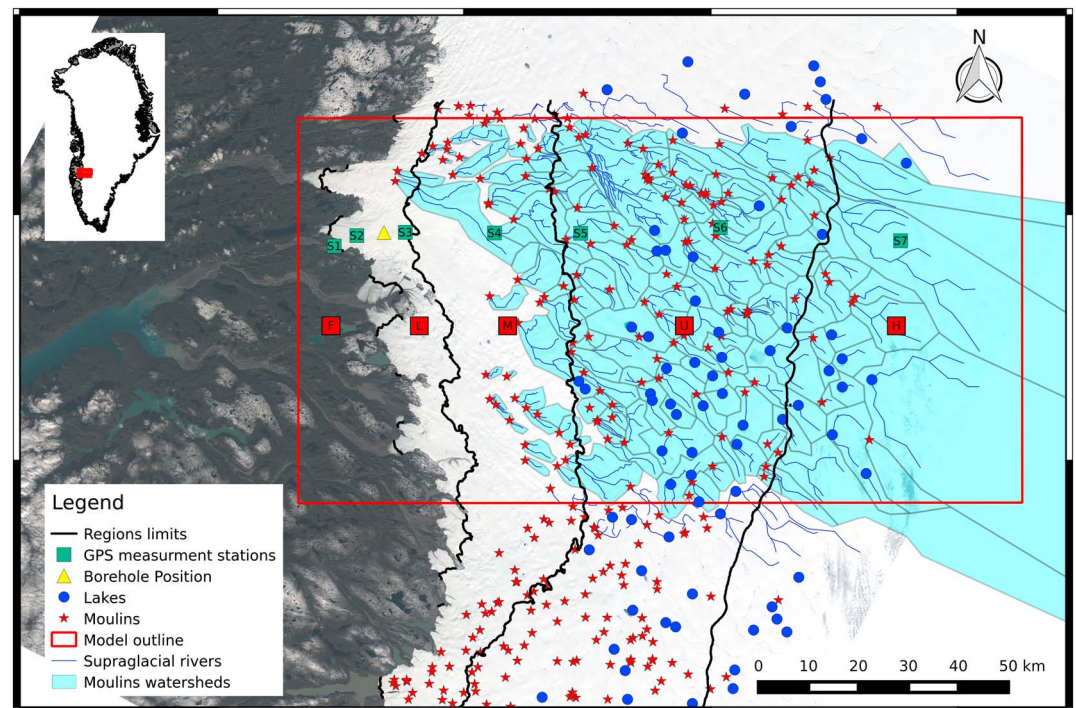


Figure 1. Map of Russell Glacier, in West Greenland, with the model outline (red rectangle), the location of moulins (red stars), and supraglacial lakes (blue dots). The supraglacial watersheds (light blue) are delineated from the supraglacial rivers (dark blue) using a Landsat 8 image from August 2013 (Landsat8_2013_231_B8) which is used as an overlay. The green squares are the locations of in situ measurements of GPS velocity presented in *Tedstone et al.* [2013] and used for comparison with the model results. The yellow triangle is the location of the SHR station where water pressure was recorded [*Smeets et al.*, 2012; *van de Wal et al.*, 2015]. The black lines are the limits of the different regions used to describe the results: the frontal region (F) below 400 m, the lower region (L) between 400 and 800 m, the median region (M) between 800 and 1200 m, the upper region (U) between 1200 and 1600 m, and finally, the highest region (H) above 1600 m.

runoff decreases, typically at the end of the summer [*Hewitt*, 2013; *Sundal et al.*, 2011; *Schoof*, 2010a]. However, sparse GPS velocities from higher-elevation areas show a persistent interannual acceleration of the ice sheet [*Doyle et al.*, 2014]. Recent studies based on remote sensing data allow to obtain the spatiotemporal resolution needed to determine the effect of subglacial hydrology on the interannual velocity of glaciers [*Tedstone et al.*, 2015], but the spatial coverage is still mostly limited to the lower part of the glacier.

Subglacial hydrological modeling may provide useful insights into the future evolution of the Greenland Ice Sheet because the models can be employed at the spatial and temporal resolutions needed to study the response of water pressure to changes in runoff. A number of subglacial hydrological models [e.g., *Werder et al.*, 2013; *de Fleurian et al.*, 2014; *Hoffman and Price*, 2014] now simulate water pressure based on our current understanding of subglacial drainage, which helps improve our understanding of the feedbacks between basal water pressure and runoff availability. These numerical models are generally designed to be coupled to higher-order ice flow models in order to include the feedback between meltwater availability and glacier dynamics. Previous studies on both synthetic [e.g., *Pimentel and Flowers*, 2010; *Schoof*, 2010b] and real cases [e.g., *Bougamont et al.*, 2014] have already shown the capability of these models to improve our knowledge of the interactions between surface runoff and glacier dynamics.

In this study, we focus on the modeling of subglacial water pressure without coupling the hydrological model with a numerical ice flow model. Our objective is to investigate the effect of interannual runoff volume variability on water pressure at the glacier base. By doing so, we avoid the difficulty of introducing a friction law in our modeling scheme that adds complexity to the analysis. We base our study on the Russell Glacier region in West Greenland, where surface mass balance models [*van de Wal et al.*, 2012] are well constrained by in situ data. The computed mass balance then allows to reconstruct runoff needed for the forcing of the subglacial hydrology model. This region also provides reliable displacement data [*Tedstone et al.*, 2013] and water

pressure measurements [Smeets *et al.*, 2012], which are used to assess the reliability of the hydrological model output (Figure 1). The subglacial hydrological model is based on the double-continuum approach described in *de Fleurian et al.* [2014] with improvements on the treatment of the efficient component of the drainage system. The effective pressure computed by the model is compared to GPS measurements of vertical displacements to evaluate the model and its parameters. Finally, we discuss on the role of runoff in controlling basal water pressure and explain how the glacier responds dynamically depending on the state of the subglacial hydrological system.

2. Methods

2.1. Subglacial Hydrological Model

Our subglacial hydrological model is based on a double-continuum approach developed by *Teutsch and Sauter* [1991] to model karstic hydrology and adapted to glaciological applications in *de Fleurian et al.* [2014]. This approach uses two porous layers to model both the inefficient (or distributed) and efficient (or channelized) components of the subglacial hydrological system (Figure 2). The two components of the system are referred to as the Inefficient Drainage System (IDS) to model the distributed part of the system and the Equivalent Porous Layer (EPL) to model the efficient drainage subsystem (Figure 2). The computation of the water heads (h_j) in the two systems is achieved by solving a vertically integrated diffusion equation:

$$S_j \frac{\partial h_j}{\partial t} - \nabla \cdot (\mathbf{T}_j \nabla h_j) = Q_j \quad (1)$$

where the subscript j represents either the IDS ($j = i$) or the EPL ($j = e$). The physical characteristics of the two layers, transmitivities \mathbf{T}_j and storing coefficients S_j , are defined as

$$\mathbf{T}_j = e_j \mathbf{K}_j, \quad (2)$$

$$S_j = e_j \rho_w \omega_j g \left[\beta_w + \frac{\alpha}{\omega_j} \right], \quad (3)$$

where e_j and \mathbf{K}_j are the thickness and conductivity of IDS or EPL, respectively. The other parameters are material characteristics of the porous media (porosity ω_j and compressibility α) and of water (density ρ_w and compressibility β_w), and g is the acceleration due to gravity.

The source term Q_j is treated in different ways depending on the system considered. Water forcing is applied only to the inefficient component of the drainage system, whereas the source for the efficient drainage system is a transfer term in between the two systems.

$$Q_i = Q - Q_t, \text{ and } Q_e = Q_t, \quad (4)$$

where Q is the forcing input discussed in section 2.2 and Q_t is the transfer flux between the two layers, which is driven by the water head difference of the two systems as

$$Q_t = \gamma(h_i - h_e), \quad (5)$$

where γ is the leakage time defining the efficiency of the coupling of the two systems.

The major difference between IDS and EPL, apart from the parameter values and the water input source, is that the IDS is always active, whereas the EPL has a specific activation procedure. The EPL is activated when the local effective pressure (computed as the difference between water pressure and ice overburden pressure) drops to zero. Upon activation, the boundary condition of the EPL region is defined as a no-flow boundary which, considering mass conservation in the system, tends to propagate the opening of the EPL downstream (i.e., following the IDS gradient). When the opening of the EPL reaches the glacier front, the same Dirichlet boundary condition as the one used for the IDS applies.

More details about this model are provided in *de Fleurian et al.* [2014]. For this study, the double-continuum approach has been implemented in the Ice Sheet System Model [Larour *et al.*, 2012], along with a new scheme to control the evolution of the thickness of the EPL. This improvement was required in order to allow for the

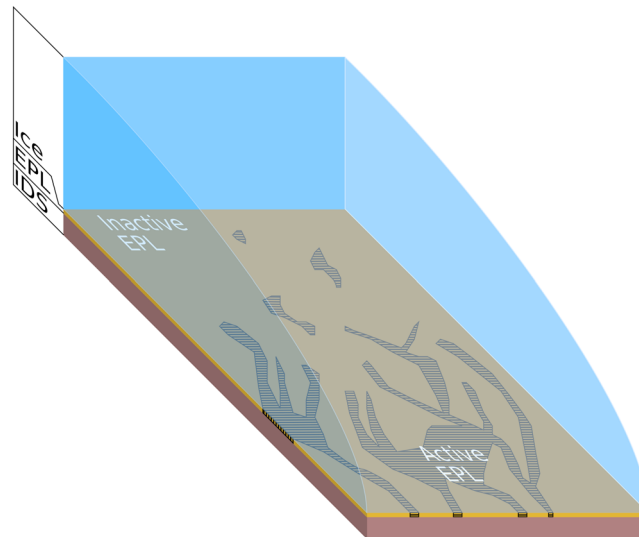


Figure 2. Conceptual diagram of the double-continuum approach. The dark and light brown layers are, respectively, the Inefficient Drainage System (IDS) and inactive Equivalent Porous Layer (EPL). The shaded region of the EPL represents its active region. This diagram presents the model applied to an idealized ice sheet (blue) with the ice flow from left to right.

collapse of the EPL at the end of the melt season, which is necessary to perform multiannual simulations. The thickness of the EPL is defined at its activation (e_j value for the EPL given in Table 1) and then left free to evolve. The thickness evolution is based on the equations developed for the computation of the size of a subglacial channel [Röthlisberger, 1972; Nye, 1976].

Computation of the size of a subglacial channel involves a widening term due to the melting of the channel walls in contact with water and a closing term due to the creeping of ice into the channel cavity. Using the equation developed by Röthlisberger [1972] for the computation of the cross section of a channel and scaling it to our specific geometry and fluxes, we obtain the following equation to describe the evolution of the EPL thickness:

$$\frac{\partial e_e}{\partial t} = \frac{g\rho_w e_e \mathbf{K}_e}{\rho_{ice} L} (\nabla h_e)^2 - 2An^{-n} N^n e_e, \tag{6}$$

where ρ_{ice} and L are the density and latent heat of fusion for the ice, respectively, N is the effective pressure, and A and n are the parameters of Glen’s flow law. A collapsing thickness (e_{col}) is introduced in the model to define a threshold below which the EPL will be deactivated. Introducing this new feature in the model makes it possible to model multiannual cycles of water head variations, which, coupled to simulated water input, enables us to study the interactions between surface runoff and water pressure at the base of glaciers.

2.2. Hydrological Forcing

Water input for the subglacial hydrological system comes from two different sources: a basal source and a surface source. The basal input is due to the geothermal and frictional heat fluxes which, by melting the ice, generate a relatively small amount of water. The surface input is driven by surface runoff, which is routed supraglacially and then englacially to the bed of the glacier. In Greenland, the surface source is the main contributor to the subglacial drainage system on the lower part of the ice sheet. However, in the interior,

Parameter	Description	IDS Value	EPL Value
e_j	layer thickness	20 m	5.0×10^{-3} m
\mathbf{K}_j	conductivity	1.0×10^{-4} m s ⁻¹	1.0×10^2 m s ⁻¹
ω_j	porosity	0.4	0.4
α	compressibility of the solid	1.0×10^{-8} Pa ⁻¹	1.0×10^{-8} Pa ⁻¹
γ	leakage time	5.0×10^{-10} s ⁻¹	5.0×10^{-10} s ⁻¹

the basal source dominates. The surface source is more critical for this study as it presents both an intraannual and interannual variability due to the variability of surface runoff, the effects of which are the main interest of this study.

2.2.1. Surface Water Input

We are interested in modeling the effect of varying runoff volume on water pressure at the base of the glacier. Considering this objective, we need a forcing that captures both the intraannual and interannual variability of the runoff. The runoff itself is well reconstructed by regional atmospheric climate models that give both reliable and extensive (in terms of space and time) time series of water production. These inputs, however, need to be preprocessed before being used as source terms in the hydrological model. The water input is here derived from runoff reconstructed by RACMO2.3 (Regional Atmospheric Climate MOdel) [Noel *et al.*, 2015]. The locations of the input points are determined from the detection of supraglacial moulins and rivers on a Landsat 8 image. More information on the preparation of the forcing is provided in Appendix A.

2.2.2. Basal Water Input

As it is less critical for the hydrological system due to its small contribution to the overall water input, the basal water source is treated in a simpler way. The geothermal heat flux is assumed to be homogeneous and constant in time over our study region with a value of 56 mW m^{-2} , which is consistent with prior studies [Fox Maule *et al.*, 2009; Dahl-Jensen *et al.*, 1998]. The other basal source, which is due to frictional heat, is ignored in this study as we are not running a coupled model, which would provide the required values of basal velocities. This second term would increase water production in the fast-flowing region of the glacier. The induced feedback is still to be studied in detail, but the small amount of water that would be generated in a region where the drainage system is already well developed should not have a significant impact on the overall effective pressure.

2.3. Model Setup

The lack of data to describe the subglacial hydrological system makes it difficult to set both the initial and boundary conditions of the model. While we focus our study on the Russell Glacier, we do not limit the model domain to the glacier catchment region, we define a larger zone of interest to make sure that the runoff of neighboring regions, which is routed subglacially to Russell Glacier, is also taken into account (Figure 1). The geometry of the glacier surface is taken from the Greenland Ice Mapping Project digital elevation model (GIMP DEM) [Howat *et al.*, 2014], and the bedrock topography is from the mass conservation method by Morlighem *et al.* [2014]. We rely on an unstructured, nonuniform mesh with characteristic element size ranging from 250 to 2500 m with an hourly time step. Ice dynamics and changes in ice geometry are ignored. We are aware that changes in geometry and the feedbacks between ice dynamics and the subglacial drainage system could impact the results of the hydrological model, but we choose to keep the model as simple as possible in order to isolate the effect of the runoff variation on the subglacial drainage system.

2.3.1. Initial and Boundary Conditions

Boundary conditions for the subglacial hydrological system are straightforward to define at the front of the glacier where the meltwater outlets define the altitude of the water table. There are a number of outlets in our region of interest, which are visible on satellite imagery and were mapped by Lewis and Smith [2009]. At these locations, the water heads of both the inefficient and efficient systems are fixed at the flotation limit. All the other boundaries of the modeled region are treated as no-flow boundaries. On the upstream boundary (where the surface elevation reaches 1850 m), this hypothesis is motivated by the fact that our domain extends to the altitude where the bed is assumed to be frozen and is thus not producing meltwater [Poinar *et al.*, 2015].

No measurement exists to constrain the initial condition of the model. To initialize the model, we use a spin-up procedure that forces the model with the time series of runoff during 2008 and repeat this yearly forcing until the model reaches a periodic state; i.e., the variations of effective pressure throughout the simulation are reproduced from year to year.

2.3.2. Parameter Selection

The material and physical parameters of the model are given in Table 2. For the hydrological parameters, the selection is difficult. This is a result of a lack of data to constrain the physical parameters and also of our particular modeling approach where the use of equivalent layers is based on parameters that are not measurable. Hydrological parameters were selected by fitting the model results of the 2008 simulation to the velocity recorded at three locations throughout the 2008 melt season [Bartholomew *et al.*, 2010]. Our main goal while setting the parameters is to get the correct timing for the evolution of water pressure with respect to the

Table 2. Definition and Values of the Physical and Material, Constants Variables and Parameters in the Model

Parameter	Definition	Value (Unit)
ρ_w	water density	1000 kg m ⁻³
ρ_{ice}	ice density	917 kg m ⁻³
g	gravitational acceleration	9.81 m s ⁻²
L	latent heat of fusion for the ice	3.34 × 10 ⁵ J kg ⁻¹
A	Glen's flow law parameter	4.29 × 10 ⁻²⁵ Pa ⁻³ s ⁻¹
n	Glen's flow law exponent	3
N	effective pressure	(Pa)
h_{ice}	ice thickness	(m)
μ	water viscosity	1.78 × 10 ⁻³ N s m ⁻²
V_{snow}	horizontal velocity of water through snow	(m s ⁻¹)
k	snow permeability	6.0 × 10 ⁻⁹
θ	surface slope	
κ	snow porosity	
V_{ice}	horizontal velocity of water on ice	(m s ⁻¹)
R	hydraulic radius	3.5 × 10 ⁻² m
n_m	Manning roughness coefficient	5.0 × 10 ⁻²
β_w	water compressibility	5.0 × 10 ⁻¹⁰ Pa ⁻¹
Q_j	source term	(m ³ s ⁻¹)
Q	runoff forcing	(m ³ s ⁻¹)
Q_t	transfer flux	(m ³ s ⁻¹)

velocity variations observed in 2008. The hydrological parameters chosen for the simulation are listed in Table 1. This fitting procedure is one of the limitations of our model; however, sensitivity studies conducted in a prior study [de Fleurian *et al.*, 2014] showed a reasonable robustness of the model results to significant changes in model parameters.

3. Data

To evaluate the model results, we use an extensive data set of GPS measurements at the surface of the glacier. This data set consists of seven stations (S1 to S7 in Figure 1) which were deployed in spring 2009 and recorded the movement of the glacier until spring 2013. Sole *et al.* [2013] and Tedstone *et al.* [2013] describe the acquisition method. From the full GPS displacement, we use only the vertical displacement recorded at each station. The measurement itself is averaged as a daily mean and linearly detrended to subtract the evolution of the station elevation as it moves downstream. The vertical displacements of stations S2 to S7 are shown in Figure 3 with the reference set at an arbitrary elevation.

To complement these velocity observations, we use the pressure data recorded in a borehole on the lower part of Russell Glacier. The position of this borehole (SHR station on the *K* transect) is indicated by the yellow triangle in Figure 1. The details on the sensors and installation are found in Smeets *et al.* [2012] and van de Wal *et al.* [2015]. The measurements started in July 2010, and we compare the daily mean to the model results.

In order to produce model results that are qualitatively comparable to the vertical displacements observed on the glacier, we extract the water pressure from the model as a Flotation Fraction (FF) which is commonly used in glaciology and defined as the ratio of water pressure over ice overburden pressure ($p_w/(\rho_{ice}gh_{ice})$) with h_{ice} the ice thickness.

4. Results

4.1. Local Evolution of the Water Pressure

We first compare the model results (in terms of FF) and the observed vertical displacements at the surface of the glacier. We chose to compare the modeled FF to the detrended daily mean vertical displacement. The vertical displacement is a good indicator of the hydraulic ice bed separation which is directly related

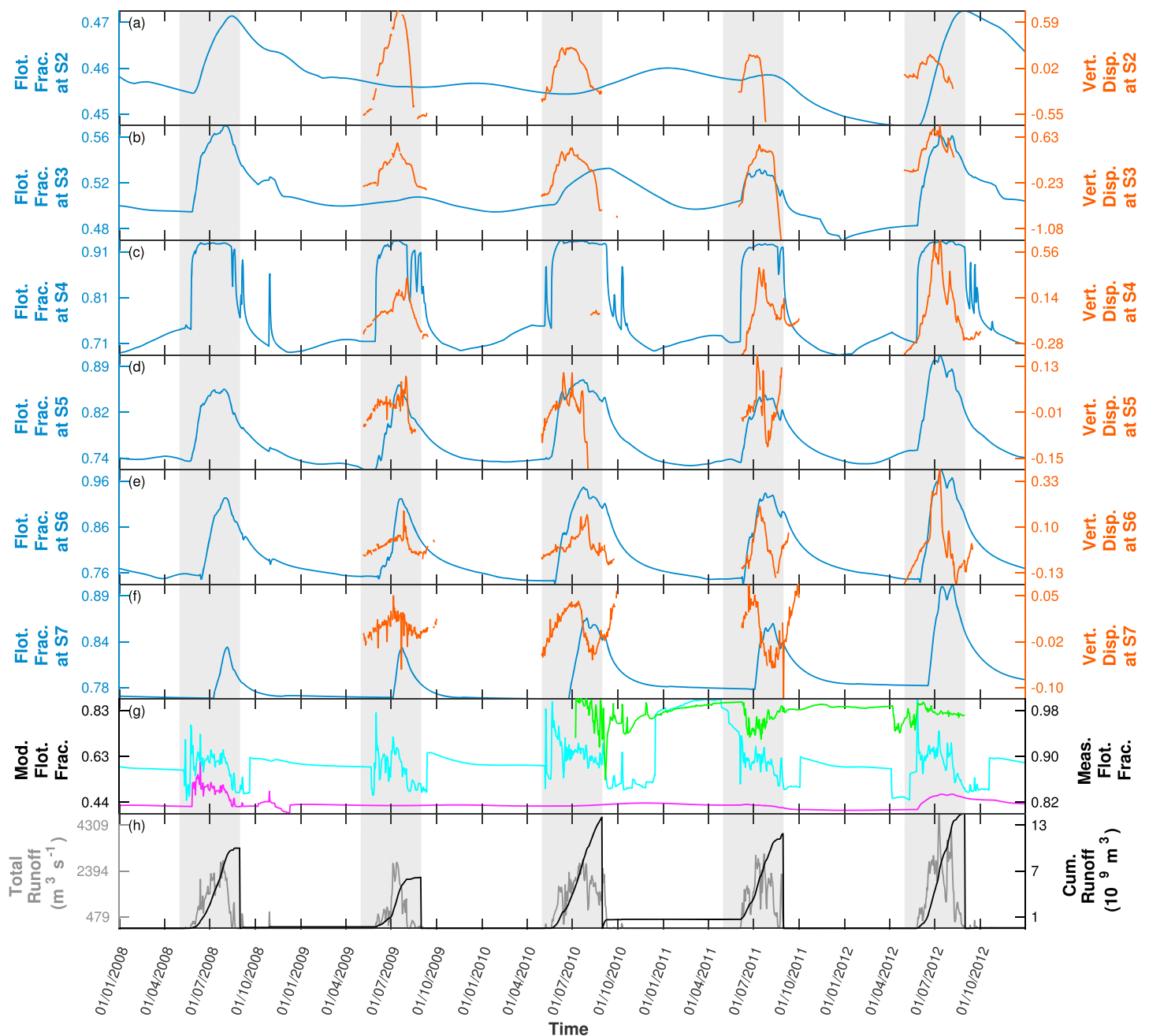


Figure 3. (a–f) Evolution of the Flotation Fraction (FF, blue left axis) and the detrended GPS measurement of vertical displacement (Vert. Disp., red right axis) for stations S2 to S7 shown in Figure 1. (g) The comparison between the measured FF (green curve right axis) at station SHR (yellow triangle in Figure 1) and the modeled FF at the same point (magenta, left axis) and a location at the same elevation where the EPL is developing (cyan, left axis). (h) Evolution of the integrated runoff (gray left axis) and cumulative integrated runoff (black right axis). The gray zones represent the summer period.

to an increase in subglacial water pressure [e.g., Iken and Bindshadler, 1986]. This comparison (Figure 3) shows a good qualitative agreement between the model and the observed displacements on a multiannual simulation. We note that there is a lag between the model and the measurements at station S7 and a very low response of the model at station S2.

To complement these observations, we compare the FF to the measured daily mean FF at the SHR station on the K transect (yellow triangle in Figure 1) [Smeets et al., 2012; van de Wal et al., 2015]. For this comparison, we use the IDS pressure when the EPL is inactive and the EPL pressure when it is active. Comparison between the measured pressure (green curve in Figure 3g) and the modeled pressure at the same location (magenta) shows

a poor agreement due to the fact that no EPL develops in this region according to the model. The comparison with a second point located at the same surface elevation but at a location where the EPL develops (cyan) gives a better agreement with the observations. The steps observed in the modeled FF are due to the pressure difference in the two systems, which appears at the activation and closure of the EPL. The modeled FF where the EPL occurs shows a good agreement with the measured FF in terms of timing of the response. There is, however, a significant difference in amplitude, with a larger amplitude of the signal for the modeled FF.

The evolution of the FF makes it possible to investigate the effect of higher meltwater quantities on the interannual evolution of the water pressure. The cumulative runoff integrated over the entire domain (Figure 3h, black curve) shows the significant amount of meltwater that is available during the melt season of 2010 and 2012. The runoff integrated over the entire domain (Figure 3h, gray curve) shows the differences between these melt seasons, 2010 being an average year in terms of amplitude but sustained over a long period, while 2012 had an amplitude higher than normal. These two situations lead to different evolutions for the FF: in 2010, the water pressure reaches a value in the range of the previous years that lasts a long period, whereas in 2012, the FF is higher than the one that was modeled for the previous melt seasons.

4.2. Global Evolution of the Water Pressure in 2010

The FF at different times in the 2010 melt season, along with the differences to the mean winter FF and the thickness of the EPL, is presented in Figure 4. An animation of the full simulation is available in the supporting information (Movie S1). The state of the model at the end of winter (10 April in Figure 4) is representative of the mean winter values as shown by the small difference between the FF at this date and the mean winter FF. The FF computed by the model is high at the glacier front, which is forced either by the boundary condition fixing the water head at the flotation limit or small ice thickness. Away from these outlets, the FF drops to more plausible values and then increases with the distance from the front. The FF is higher in large troughs in the glacier bed, which indicates a preferential drainage in these areas. On the highest parts of the domain, the FF decreases as the ice thickness increases, whereas the water pressure is stable due to the lack of water influx at these altitudes. The EPL thickness, which represents the development of an efficient drainage system, shows remnants of the draining system from the preceding melt season. These remnants of an efficient drainage system are likely comparable to an unconnected water system as they have a very small thickness and are not connected to the glacier front.

During the melt season (4 June and 3 August in Figure 4) the moulins are feeding the subglacial drainage system, leading to an increase in FF on most of the domain. The FF increase starts on the lower part of the glacier with the emergence of the first moulins at lower elevation. This increase in pressure triggers the development of the EPL at these elevations, where a few well-developed channel-like structures are formed to evacuate the water. Later in the melt season, the FF increase extends over most of the model domain with only a small region at the upper limit of the domain, which is not impacted by the meltwater input. Note that the higher-pressure front is reaching a point higher than the highest moulin. On 3 August, the EPL is at its maximum extent. In this configuration, we observe a few well-developed channel-like structures on the lower part of the domain. Higher up, the drainage system is more widespread and less efficient (smaller EPL thickness) over almost all the glacier bed.

At the start of winter (12 September in Figure 4), the FF quickly decreases as a result of the presence of a now well-developed efficient drainage system and a drop in meltwater input. This drop in pressure yields a rapid decrease of the EPL thickness in the regions where no preferential drainage pathways were developed, but the major drainage pathways still present a large thickness that allows the remaining meltwater to drain.

Finally, well into fall (22 October in Figure 4), the water pressure returns to its mean winter value and the EPL thickness continues to decrease before it collapses in the middle of winter.

4.3. Interannual Variability of the Water Pressure

Performing long simulations makes it possible to investigate the interannual variations of the basal water pressure. To get a more synoptic view of the water pressure evolution throughout the years, we compute the mean value of the FF in given surface elevation bins. Figure 5 presents the FF variations for 50 m surface elevation bins throughout the simulation. The reference for each elevation bin is the mean value of the FF for all the simulated winters (mean winter value, MWV). The pattern of the FF evolution is similar from year to year with differences in the duration and amplitude of the signal. The water pressure remains at or just below the MWV for the beginning of the summer and then increases as meltwater becomes available.

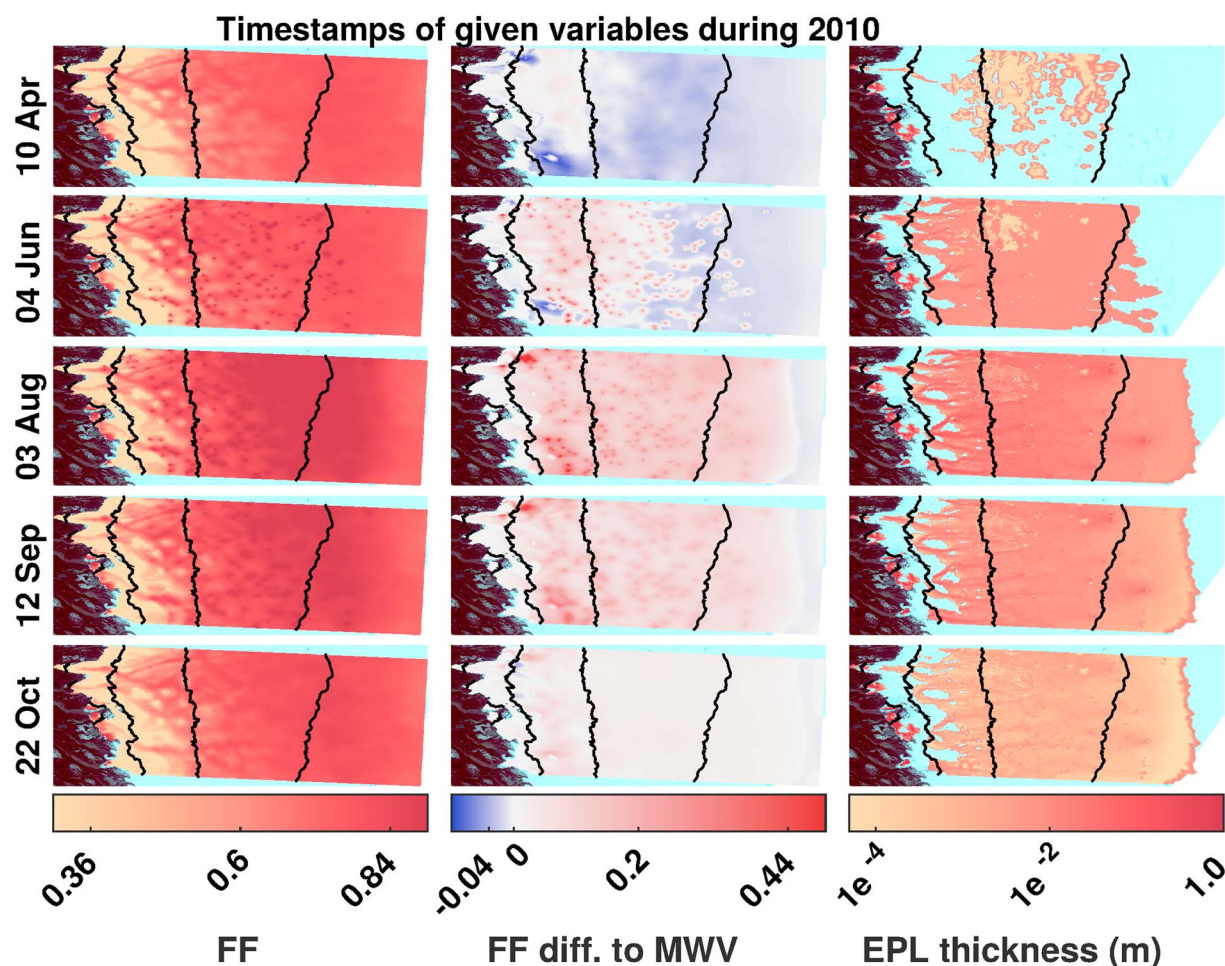


Figure 4. Maps of the Flotation Fraction (FF), its difference to the mean winter value (MWV) of the FF, and the thickness of the Equivalent Porous Layer (EPL) at different dates during the 2010 melt season. The mean winter value is defined as the mean winter FF average over all the simulated winters. The FF presents the evolution of the water pressure, whereas the thickness of the EPL represents the development of the efficient drainage system at the base of the glacier. Inactive EPL points are transparent on the third column. The results are overlaid on the same Landsat 8 image as in Figure 1. See supporting information for an animation of the complete simulation (Movie S1).

The region below 400 m elevation does not show any significant variation in water pressure. Above 400 m, there is a strong seasonal cycle in water pressure. The pressure first increases around 800 to 1200 m elevation, and then the increase in FF spreads downstream as the pressure builds up in the inefficient drainage system and upstream as the melt season goes on and a larger number of moulins feed the subglacial hydrological system. At the end of the summer, the water pressure drops to its winter level. The first place where the FF returns to its winter level is again between 800 and 1200 m elevation, where the development of an efficient drainage system allows to move the water downstream while lowering the water pressure at the base of the glacier. The winter season is marked by a lower FF, but the dynamics of the variability in FF varies across the region. Between the front of the glaciers and 800 m, the FF drops at the end of summer and then stays at the same level for the whole winter. Higher up on the domain, between 800 and 1200 m, the FF quickly drops at the end of summer to get to a low and then increases to get to the MWV at the end of winter. The behavior is reversed at higher elevation (from 1200 to 1600 m) where the FF decreases during all winter. Finally, the highest part of the glacier, above 1600 m, exhibits a different behavior with a moderate decrease of the FF during winter, which is particularly visible after the 2010 melt season.

4.4. Spatial Variability of the Water Pressure Variation

An examination of the seasonal mean of the FF provides useful insights about the long-term evolution of water pressure. From the previous results, we define regions with different responses to the runoff forcing: (1) the frontal region (from the ice margin to 400 m of elevation), (2) the lower region (from 400 to 800 m),

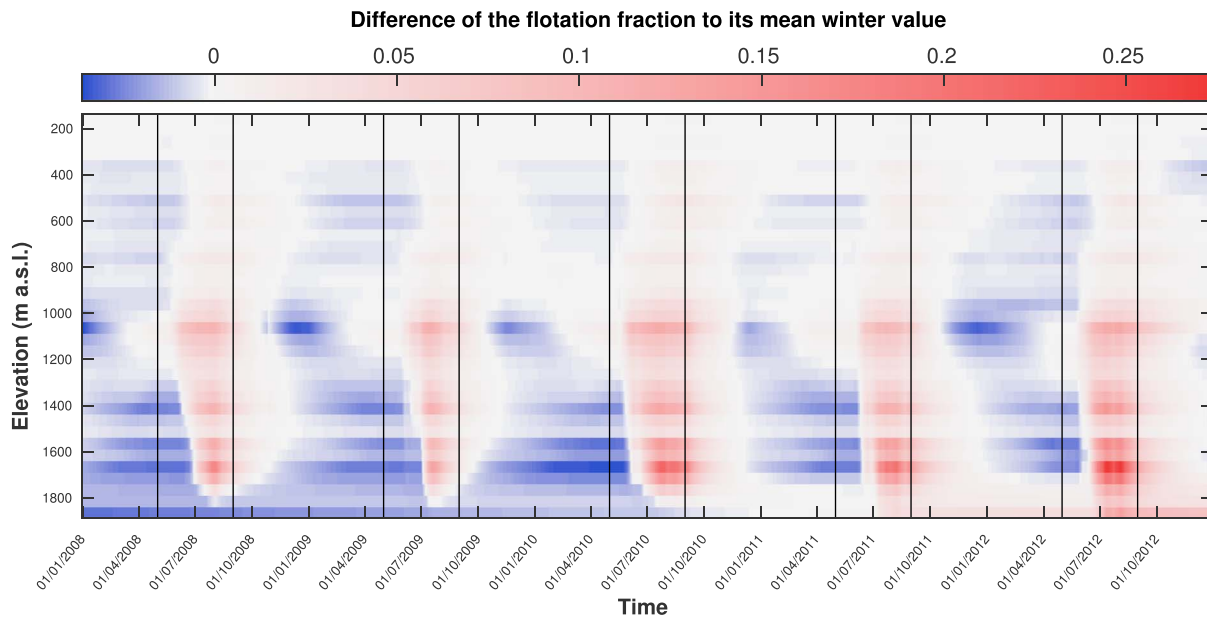


Figure 5. Evolution of the Flotation Fraction (FF) relative to the mean winter value. The mean winter value is defined as the mean winter FF average over all the simulated winters. The values presented here are averaged over 50 m elevation bins. The black lines represent the start and end of summer.

(3) the median region (from 800 to 1200 m), (4) the upper region (from 1200 to 1600 m), and (5) the highest region (from 1600 m to the top of the domain). The five regions are delineated in Figure 1.

The values presented in Figure 6 are the percentages difference of the FF seasonal means with respect to the MWV averaged over the given regions. The seasons are defined as typical for this region: the summer is from 1 May to 31 August, winter from 1 September to 30 April, and the annual mean is from 1 May to 30 April. The figure only shows the summer mean for 2012 as the simulation does not span the entire winter of 2012.

As stated before, there is no significant trend in interannual or intraannual evolution of the FF on the frontal region. The evolution is more significant on the rest of the model domain. For the period starting at the beginning of the 2008 melt season and finishing at the end of the 2009 winter, the evolution of the FF is the same for all regions with a decrease in annual FF. This decrease is triggered by lower summer FF in the lower and median regions but is mainly driven by the reduction in winter FF in the highest region. The upper region reduction of the annual FF is due to a lowering of both the summer FF and winter FF.

In 2010, which experienced a significant and sustained melt season, the FF annual means show a dramatic increase in all regions. This increase is mainly due to the increase in FF during summer, but the model results also show an increase in winter.

Year 2011 marks the return of a more average melt year with meltwater levels closer to those of year 2008. This period shows different patterns in the evolution of the FF across the region. In the lower and median regions, the summer FF is back to the level observed in 2008 but the winter mean value is lower than the previous

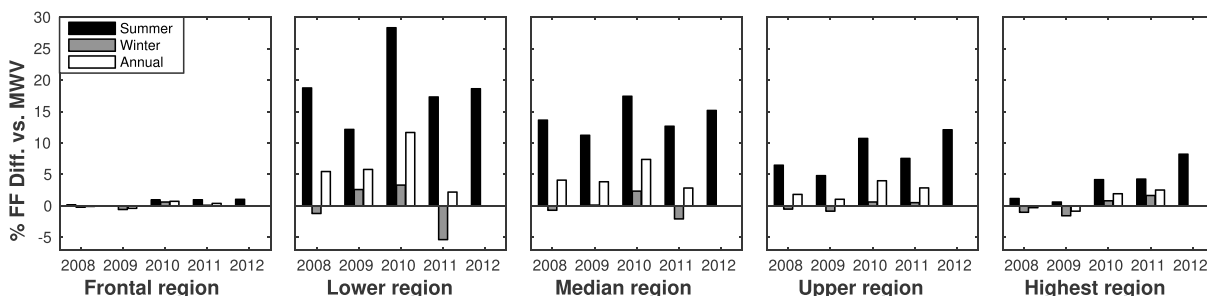


Figure 6. Percentage difference of the FF seasonal mean with respect to the MWV averaged on the different regions described in the text. The frontal (F), lower (L), median (M), upper (U), and highest (H) regions are delineated on the map in Figure 1.

years leading to a smaller mean annual FF. The evolution is rather different in the upper region: the FF mean values are more comparable to the ones modeled during 2010, with only a slight decrease in annual mean FF driven by a decrease of the summer value of the water pressure. Finally, the highest zone shows a continuous increase in FF even during this rather low input melt season.

Our model suggests that the record melt year of 2012 does not lead to extreme FF values on the lower part of our domain. The summer means are in the range of values modeled for the other years of the simulation on the lower median and upper regions. In contrast, the highest region displays a FF that increases twice as fast as during the entire modeling period.

5. Discussion

The application of a new generation, multicomponent, subglacial hydrological model provides new insight into the varying responses of the subglacial hydrological system to the evolution of the meltwater volume in Greenland. The analysis of these distinct subglacial hydrological modes is key to understanding the causes of the different velocity evolutions that are observed on Russell Glacier.

The comparison between the modeled water pressure and the measured vertical surface motion of the glacier shows a good qualitative agreement (Figure 3). The results are consistent with the data for both the seasonal and shorter time scale variations of the signal. The results at stations S2 and S7 are less convincing, which is probably due to various reasons. At station S2, the lack of evolution in the modeled water pressure is probably due to the fact that this station is close to the glacier front and still impacted by the boundary condition that is fixed at this point (Dirichlet). At the uppermost station (station S7), we are more confident in the model results, but, at this point, the ratio between surface uplift and vertical displacement due to the downstream motion of the ice is small, leading to uncertainties in the reliability of the detrended data at this location. The water pressure modeled at the SHR station is not consistent with the observations [Smeets *et al.*, 2012], which was anticipated given the fact that the EPL does not develop at this location in the model. However, the comparison with the data from a grid point where the EPL develops shows a good agreement in terms of timing of the pressure variations. The general shape of the modeled pressure also agrees reasonably well to the measured pressure, even for the late season water pulse observed during the winter of 2010. The amplitudes of the modeled pressure are higher than the measured ones, which is probably due to the rather low pressure that is modeled on the lower part of the glacier. We note that there is still a lack of velocity data during the winter season. Acquiring more data during winter as done by van de Wal *et al.* [2015] will enable a better evaluation of the models.

The modeling of a large region around the Russell Glacier catchment helps us investigate the characteristics of the drainage system in the region. The snapshots in Figure 4 and particularly the EPL thickness on 3 August give us a good idea about the characteristics of the drainage system when its efficient component is at its maximum extent. On this date, the EPL thickness shows large channel-like structures extending up to 1200 m in elevation, which is comparable to 41 to 57 km from the glacier front which was defined as the limit of the development of the efficient drainage system by Chandler *et al.* [2013]. The modeled effective system also shows a different localization from year to year as proposed by Chu *et al.* [2016]. The displacement of these major drainage pathways can be consulted in the supporting information (Movie S1). Farther upglacier, the EPL is still active but shows a smaller thickness and no channel-like structure, which is consistent with a less efficient system that would be formed by a larger network of interconnected cavities. Finally, on the highest part of the ice sheet, the EPL is nonexistent, even at the peak of the melt season, which in our model is mainly due to the fact that the water input is too low (no moulin) to allow water pressure to reach flotation level and activate the EPL. Contrary to the results from Chandler *et al.* [2013], our model shows a developed efficient system, which exists year round near the front of the glacier. This is probably caused by the imposed boundary conditions at the ice margin.

The evolution of water pressure in Figure 5 sheds light on the observed surface velocity and its link to the subglacial water pressure. Observations made in the region have shown an increase in summer velocity during the summers of 2010 and 2012 [Sole *et al.*, 2013; van de Wal *et al.*, 2015], which had a high meltwater input to the glacier. These unusually high velocities can be explained by the broader and higher water pressure peak that are modeled during these years. The model results, however, do not show a lower winter water pressure during these years as hypothesized by Pimentel and Flowers [2010] and observed by Sundal *et al.* [2011] in the lower part of the ice sheet. The FF evolution during 2010, which is the only high melt season for which we also

modeled winter values of the water pressure, yields interesting results because even with a larger melt event, the winter FF is not impacted and is similar to the FF modeled for the winters of 2008 and 2009. This result indicates that the observed lower winter velocities subsequent to extreme summer melt [Tedstone *et al.*, 2015] are probably not entirely due to the response of the subglacial drainage system. Our results, however, are only addressing the evolution of water pressure from a nonfully coupled system. A fully coupled model could yield different results due to feedbacks [Hoffman and Price, 2014; Hewitt, 2013]. Another hypothesis would be the one presented by Andrews *et al.* [2014] and Meierbachtol *et al.* [2016] about the importance of hydraulically isolated region of the beds on the variation in late season water pressure.

The results of the model in the highest part of the domain give insight into the processes leading to the distinct behavior observed when investigating the evolution of the ice velocity on this glacier. Above 1600 m, the model shows a constant increase in subglacial water pressure after 2010. This increase cannot be due to a migration of the moulins upstream as these injection points have a fixed location in space throughout the simulation. Our model results indicate that following the high meltwater forcing of the 2010 melt season, the water heads in the moulin region reached a height sufficient to invert the gradient of the hydraulic potential in the highest part of the domain. This inversion allowed the inefficient system to fill-up without reaching a volume of water necessary to build the water pressure at a level consistent with the development of an efficient drainage system. This phenomenon shows that even if there is no way for the water to reach the bed at these high elevations, the upstream propagation of a pressure wave in the inefficient drainage system has the ability to increase the subglacial water pressure in the interior of the ice sheet. These results provide an explanation for the distinct velocity regimes that are observed on the glacier. On the lower part of the glacier, the pressure builds up during the beginning of the melt season, leading to a speedup. The speedup is hindered by the development of an efficient drainage system that lowers the water pressure to values close to the mean winter value at the end of summer. This pressure drop leads to the return of the glacier velocities to their winter values. On the other hand, the buildup of pressure on the highest part of the glacier is not followed by a drop in pressure as the efficient drainage system does not develop at these altitudes.

This study has allowed to differentiate two regions in the drainage dynamics of the Russell region. In the lower part of the glacier, the water pressure is driven by an efficient drainage system which develops early in the melt season, decreases subglacial water pressure, and hence produces the surface velocities observed by Sole *et al.* [2013] and Tedstone *et al.* [2013]. The subglacial water pressure on the upper part of the glacier, however, is mostly driven by an inefficient drainage system in which the pressure builds up from one melt season to the next one. This increase in subglacial water pressure could be the source of the acceleration in surface velocity observed by Doyle *et al.* [2014] on the higher part of Russell Glacier.

The mechanism explained above still leaves uncertainties about the long-term effect of an increase in meltwater production in Greenland. Our results suggest that the water pressure on the highest part of the glacier will continue to build up if the meltwater input is sustained at its current level. This would have the effect of maintaining the interannual speedup, which is currently observed. If this process is sustained for a certain amount of time, it could build up a subglacial pressure wave with the potential to destabilize the highest part of the ice sheet as was proposed by Zwally *et al.* [2002]. Another possibility is that the increase in pressure at higher elevation leads to the development of an efficient channel system at high elevation. This development would lead to a mitigation of the interannual acceleration, and the upper part of the glacier would exhibit a more marked seasonal evolution similar to the one presently occurring below the ELA. This would necessitate the development of an efficient drainage system under thick ice, which is unlikely [Dow *et al.*, 2014] if the input of water at higher elevation is not sustained by large and sustained meltwater production.

The main limitation of our model is in the choice of its parameters that we cannot measure in the field and hence need to be fitted. Sensitivity studies performed in earlier experiments [de Fleurian *et al.*, 2014] show that the model gives consistent results in terms of variations in the timing and amplitude of water pressure when different parameter sets are used. Another problem that arose in this study is the impact of the ice margin conditions on water pressure. However, this impact seems to be limited to the lowest part of the glacier tongues, which are not very extensive and do not seem to impact the results on the remainder of the domain. The coupling of this model to an ice dynamics model should be an important objective for future studies in order to fully ascertain if the hypothesis presented herein remains valid in the case of a fully coupled system.

6. Conclusion

We model the evolution of the water pressure at the base of Russell Glacier, in West Greenland, and its neighboring glaciers for five complete melt seasons including the two extreme melt seasons of 2010 and 2012. The model is in good agreement with vertical surface displacements measured by GPS stations. The double-continuum approach also shows a good agreement with the configuration of the subglacial drainage system as described from dye and gas tracer tests performed by *Chandler et al.* [2013]. The results confirm the observations from *Doyle et al.* [2014] of an acceleration of the interior part of the Greenland Ice Sheet but reconcile these results with those obtained by *Tedstone et al.* [2013] on the lower part of the glacier where the higher melt rate had only a limited impact on the dynamic of the ice sheet. On this last point, the model results are not as definitive as the observations and we cannot ascertain that the larger melt rate would lead to smaller water pressure during winter. However, even if these results are not present in our simulations, we hypothesize that this is due to the coupling mechanism of the model, not to a flaw in the subglacial hydrological model. This study shows that the development of an efficient drainage system is key in the evolution of water pressure at the base of glaciers, which in turn is essential to understand the observed difference in velocity regime. Further studies will be needed to evaluate the migration speed of the efficient system upper limit, which controls the position of the boundary between the two distinct water pressure modes of behavior. Data collection should continue and be repeated in these regions to observe the migration of the upper boundary of the efficient drainage system with time.

Appendix A: Hydrological Forcing Description

Our subglacial hydrological model does not take into account the supraglacial and englacial components of the hydrological system. This means that we need to specify the recharge points of the system. We make the assumption that the moulin shafts, which are spotted at the surface of the glacier, are vertical enough so that their position at the surface is matching the recharge point of the subglacial hydrological system. Following this assumption, we have located the moulins on our modeling domain which will correspond to the injection point for the hydrological model (Figure 1).

As the modeled area is not very extensive, we manually picked the moulins on a Landsat 8 image from late summer 2013. The selection of the image has been done as late as possible during the melt season to display the most developed supraglacial river network. Each visible river has then been plotted, and considering that every river ends up in a moulin or a lake [*Smith et al.*, 2015], these were placed at the end of the precedingly drawn rivers.

The comparison of our mapping with the much more advanced one made in the region by *Smith et al.* [2015] shows a good coherence. However, we decided to keep our map as the spatial coverage of their study was not overlapping all of our model domain. The plotted moulins are kept at the same position throughout the simulation period. We do not account for the displacement of the moulins with the encompassing ice or the creation of new moulins. This assumption could be problematic when looking at an inland increase in surface runoff that generates new moulins farther upglacier. Considering this issue, we chose to identify our injection point on an image taken after the record melt year of 2012 to allow for the injection of water in newly formed moulins.

The discharge in each moulin that have been plotted earlier is the integration of the runoff values over the moulin catchment area. The catchment of each moulin is defined by the river network that ends in this moulin. For the upper moulins, where no river is present at the surface of the ice sheet, the watersheds have been extended to the limit of the domain following the slope of the Greenland Ice Mapping Project (GIMP) DEM [*Howat et al.*, 2014]. The resulting map containing the moulins and their related rivers and catchment is presented in Figure 1.

The generation of this supraglacial hydrological map creates an interface between the surface runoff computed by the RACMO model and the subglacial hydrological model. The forcing from the daily RACMO2.3 runoff is then computed at each moulin location. The moulin input is computed considering the integrated runoff on its watershed and the transfer time from the runoff point to the moulin position. Transfer time depends on the surface slope, which is computed from the GIMP DEM and from the surface cover (snow or ice). The presence of snow is derived from the surface mass balance from the RACMO2.3 simulation. If snow is present, the RACMO2.3 runoff corresponds to the deep runoff at the interface between ice and snow,

and the water velocity (V_{snow}) to be taken into account is then only the velocity of the water flowing in a saturated snowpack as defined by Colbeck [1978]:

$$V_{\text{snow}} = \left(\frac{\rho_w g}{\mu} \right) \frac{k\theta}{\kappa}, \quad (\text{A1})$$

where μ is the water viscosity, θ is the surface slope, and finally, k and κ are respectively the permeability and porosity of snow, which are given by a RACMO2-driven firn model on a weekly basis [Kuipers Munneke et al., 2015]. For the bare ice region, the Manning formula is used to compute V_{ice} , the water velocity at the surface of the ice sheet, as

$$V_{\text{ice}} = \frac{R^{2/3}\theta^{1/2}}{n_m}, \quad (\text{A2})$$

where R and n_m are respectively the hydraulic radius of the supraglacial channel and the Manning roughness coefficient.

From these two equations, the time necessary for the water to cover the distance from its production site to the moulin is calculated and the daily sum of all the inputs for a given watershed is used to force the subglacial hydrological model.

Acknowledgments

This work was performed at the University of California Irvine and at the California Institute of Technology's Jet Propulsion Laboratory under a contract with the National Aeronautics and Space Administration. We acknowledge data from NASA's Operation IceBridge mission. Request for data should be made respectively to C.J.P.P. Smeets (C.J.P.P.Smeets@uu.nl) for pressure data at SHR, M.R. van den Broeke (M.R.vandenBroeke@uu.nl) for RACMO2 output, and P.W. Nienow (pnieow@staffmail.ed.ac.uk) for GPS velocities on Russell Glacier. We thank the reviewers for their constructive comments that helped to improve the manuscript quality.

References

- Andrews, L. C., G. A. Catania, M. J. Hoffman, J. D. Gulley, M. P. Luethi, C. Ryser, R. L. Hawley, and T. A. Neumann (2014), Direct observations of evolving subglacial drainage beneath the Greenland Ice Sheet, *Nature*, *514*(7520), 80–83, doi:10.1038/nature13796.
- Bartholomew, I., P. Nienow, D. Mair, A. Hubbard, M. A. King, and A. Sole (2010), Seasonal evolution of subglacial drainage and acceleration in a Greenland outlet glacier, *Nat. Geosci.*, *3*(6), 408–411, doi:10.1038/NGEO863.
- Bougamont, M., P. Christoffersen, A. L. Hubbard, A. A. Fitzpatrick, S. H. Doyle, and S. P. Carter (2014), Sensitive response of the Greenland ice sheet to surface melt drainage over a soft bed, *Nat. Commun.*, *5*, 5052, doi:10.1038/ncomms6052.
- Chandler, D. M., et al. (2013), Evolution of the subglacial drainage system beneath the Greenland Ice Sheet revealed by tracers, *Nat. Geosci.*, *6*(3), 195–198, doi:10.1038/ngeo1737.
- Chu, W., T. T. Creyts, and R. E. Bell (2016), Rerouting of subglacial water flow between neighboring glaciers in West Greenland, *J. Geophys. Res. Earth Surf.*, *121*(5), 925–938, doi:10.1002/2015JF003705.
- Colbeck, S. (1978), The physical aspects of water flow through snow, *Adv. Hydrol.*, *11*, 165–206, doi:10.1016/B978-0-12-021811-0.50008-5.
- Cuffey, K., and W. S. B. Paterson (2010), *The Physics of Glaciers*, 4th ed., Elsevier, Oxford.
- Dahl-Jensen, D., K. Mosegaard, N. Gundestrup, G. Clow, S. Johnsen, A. Hansen, and N. Balling (1998), Past temperatures directly from the Greenland Ice Sheet, *Science*, *282*(5387), 268–271, doi:10.1126/science.282.5387.268.
- de Fleurian, B., O. Gagliardini, T. Zwinger, G. Durand, E. Le Meur, D. Mair, and P. Råback (2014), A double continuum hydrological model for glacier applications, *Cryosphere*, *8*(1), 137–153, doi:10.5194/tc-8-137-2014.
- Dow, C. F., B. Kulesa, I. C. Rutt, S. H. Doyle, and A. Hubbard (2014), Upper bounds on subglacial channel development for interior regions of the Greenland ice sheet, *J. Glaciol.*, *60*(224), 1044–1052, doi:10.3189/2014JoG141093.
- Doyle, S. H., A. Hubbard, A. A. W. Fitzpatrick, D. van As, A. B. Mikkelsen, R. Pettersson, and B. Hubbard (2014), Persistent flow acceleration within the interior of the Greenland ice sheet, *Geophys. Res. Lett.*, *41*(3), 899–905, doi:10.1002/2013GL058933.
- Engelhardt, H., and B. Kamb (1998), Basal sliding of Ice Stream B, West Antarctica, *J. Glaciol.*, *44*(147), 223–230.
- Flowers, G. E. (2017), Modelling water flow under glaciers and ice sheets, *Proc. R. Soc. London, Ser. A*, *471*, 1–41, doi:10.1098/rspa.2014.0907.
- Fox Maule, C., M. E. Purucker, and N. Olsen (2009), Inferring magnetic crustal thickness and geothermal heat flux from crustal magnetic field models, Tech. Rep. 09–09, Danish Meteorol Inst., Denmark.
- Hewitt, I. J. (2013), Seasonal changes in ice sheet motion due to melt water lubrication, *Earth Planet. Sci. Lett.*, *371*–372, 16–25, doi:10.1016/j.epsl.2013.04.022.
- Hewitt, I. J., and A. C. Fowler (2008), Seasonal waves on glaciers, *Hydrol. Process.*, *22*(19), 3919–3930.
- Hoffman, M., and S. Price (2014), Feedbacks between coupled subglacial hydrology and glacier dynamics, *J. Geophys. Res. Earth Surf.*, *119*(3), 414–436, doi:10.1002/2013JF002943.
- Howat, I. M., A. Negrete, and B. E. Smith (2014), The Greenland Ice Mapping Project (GIMP) land classification and surface elevation datasets, *Cryosphere*, *8*(4), 1509–1518, doi:10.5194/tc-8-1509-2014.
- Iken, A., and R. A. Bindschadler (1986), Combined measurements of subglacial water-pressure and surface velocity of Findelengletscher, Switzerland, *J. Glaciol.*, *32*(110), 101–119.
- Iken, A., K. Echelmeyer, W. Harrison, and M. Funk (1993), Mechanisms of fast flow in Jakobshavns-Isbrae, West Greenland: 1. Measurements of temperature and water-level in deep boreholes, *J. Glaciol.*, *39*(131), 15–25.
- Kamb, B., C. F. Raymond, W. D. Harrison, H. Engelhardt, K. A. Echelmeyer, N. Humphrey, M. M. Brugman, and T. Pfeffer (1985), Glacier surge mechanism: 1982–1983 surge of Variegated Glacier, Alaska, *Science*, *227*(4686), 469–479, doi:10.1126/science.227.4686.469.
- Larour, E., H. Seroussi, M. Morlighem, and E. Rignot (2012), Continental scale, high order, high spatial resolution, ice sheet modeling using the Ice Sheet System Model (ISSM), *J. Geophys. Res.*, *117*(F01022), 1–20, doi:10.1029/2011JF002140.
- Lewis, S. M., and L. C. Smith (2009), Hydrologic drainage of the Greenland ice sheet, *Hydrol. Process.*, *23*(14), 2004–2011, doi:10.1002/hyp.7343.
- Luthi, M., M. Funk, A. Iken, S. Gogineni, and M. Truffer (2002), Mechanisms of fast flow in Jakobshavn Isbrae, West Greenland: Part III. Measurements of ice deformation, temperature and cross-borehole conductivity in boreholes to the bedrock, *J. Glaciol.*, *48*(162), 369–385, doi:10.3189/172756502781831322.
- Meierbachtol, T. W., J. T. Harper, N. F. Humphrey, and P. J. Wright (2016), Mechanical forcing of water pressure in a hydraulically isolated reach beneath Western Greenland's ablation zone, *Ann. Glaciol.*, 1–9, doi:10.1017/aog.2016.5.
- Morlighem, M., H. Seroussi, E. Larour, and E. Rignot (2013), Inversion of basal friction in Antarctica using exact and incomplete adjoints of a higher-order model, *J. Geophys. Res. Earth Surf.*, *118*(3), 1746–1753, doi:10.1002/jgrf.20125.

- Morlighem, M., E. Rignot, J. Mouginot, H. Seroussi, and E. Larour (2014), Deeply incised submarine glacial valleys beneath the Greenland Ice Sheet, *Nat. Geosci.*, 7(6), 418–422, doi:10.1038/ngeo2167.
- Kuipers Munneke, P., et al. (2015), Elevation change of the Greenland Ice Sheet due to surface mass balance and firn processes, 1960–2014, *Cryosphere*, 9(6), 2009–2025, doi:10.5194/tc-9-2009-2015.
- Noel, B., W. J. van de Berg, E. van Meijgaard, P. Kuipers Munneke, R. S. W. van de Wal, and M. R. van den Broeke (2015), Evaluation of the updated regional climate model RACMO2. 3: Summer snowfall impact on the Greenland Ice Sheet, *Cryosphere*, 9(5), 1831–1844, doi:10.5194/tc-9-1831-2015.
- Nye, J. (1976), Water flow in glaciers: Jokulhlaups, tunnels and veins, *J. Glaciol.*, 17(76), 181–207.
- Palmer, S., A. Shepherd, P. Nienow, and I. Joughin (2011), Seasonal speedup of the Greenland Ice Sheet linked to routing of surface water, *Earth Planet. Sci. Lett.*, 302(3–4), 423–428, doi:10.1016/j.epsl.2010.12.037.
- Pimentel, S., and G. E. Flowers (2010), A numerical study of hydrologically driven glacier dynamics and subglacial flooding, *Proc. R. Soc. A*, 467(2126), 537–558, doi:10.1098/rspa.2010.0211.
- Poinar, K., I. Joughin, S. Das, M. Behn, J. Lenaerts, and M. van den Broeke (2015), Limits to future expansion of surface-melt-enhanced ice flow into the interior of western Greenland, *Geophys. Res. Lett.*, 42, 1800–1807, doi:10.1002/2015GL063192.
- Röthlisberger, H. (1972), Water pressure in intra- and subglacial channels, *J. Glaciol.*, 11(62), 177–203.
- Schoof, C. (2010a), Coulomb friction and other sliding laws in a higher-order glacier flow model, *Math. Models Methods Appl. Sci.*, 20(1), 157–189, doi:10.1142/S0218202510004180.
- Schoof, C. (2010b), Ice-sheet acceleration driven by melt supply variability, *Nature*, 468(7325), 803–806, doi:10.1038/nature09618.
- Smeets, C. J. P. P., W. Boot, A. Hubbard, R. Pettersson, F. Wilhelms, M. R. van den Broeke, and R. S. W. van de Wal (2012), A wireless subglacial probe for deep ice applications, *J. Glaciol.*, 58(211), 841–848, doi:10.3189/2012JoG11J130.
- Smith, L. C., et al. (2015), Efficient meltwater drainage through supraglacial streams and rivers on the Southwest Greenland ice sheet, *Proc. Natl. Acad. Sci.*, 112(4), 1001–1006, doi:10.1073/pnas.1413024112.
- Sole, A., P. Nienow, I. Bartholomew, D. Mair, T. Cowton, A. Tedstone, and M. A. King (2013), Winter motion mediates dynamic response of the Greenland Ice Sheet to warmer summers, *Geophys. Res. Lett.*, 40(15), 3940–3944, doi:10.1002/grl.50764.
- Sundal, A. V., A. Shepherd, P. Nienow, E. Hanna, S. Palmer, and P. Huybrechts (2011), Melt-induced speed-up of Greenland ice sheet offset by efficient subglacial drainage, *Nature*, 469(7331), 522–524, doi:10.1038/nature09740.
- Tedstone, A. J., P. W. Nienow, A. J. Sole, D. W. F. Mair, T. R. Cowton, I. D. Bartholomew, and M. A. King (2013), Greenland ice sheet motion insensitive to exceptional meltwater forcing, *Proc. Natl. Acad. Sci.*, 110(49), 19,719–19,724, doi:10.1073/pnas.1315843110.
- Tedstone, A. J., P. W. Nienow, N. Gourmelen, A. Dehecq, D. Goldberg, and E. Hanna (2015), Decadal slowdown of a land-terminating sector of the Greenland Ice Sheet despite warming, *Nature*, 526(7575), 692–695, doi:10.1038/nature15722.
- Teutsch, G., and M. Sauter (1991), Groundwater modeling in karst terranes: Scale effects, data acquisition and field validation, in *Third Conference on Hydrogeology, Ecology, Monitoring, and Management of Ground Water in Karst Terranes*, pp. 17–35, National Ground Water Association, Dublin, Ohio.
- van de Wal, R. S. W., W. Boot, C. J. P. P. Smeets, H. Snellen, M. R. van den Broeke, and J. Oerlemans (2012), Twenty-one years of mass balance observations along the K-transect, West Greenland, *Earth Syst. Sci. Data*, 4, 31–25.
- van de Wal, R. S. W., et al. (2015), Self-regulation of ice flow varies across the ablation area in south-west Greenland, *Cryosphere*, 9(2), 603–611, doi:10.5194/tc-9-603-2015.
- Werder, M. A., I. J. Hewitt, C. G. Schoof, and G. E. Flowers (2013), Modeling channelized and distributed subglacial drainage in two dimensions, *J. Geophys. Res. Earth Surf.*, 118, 1–19, doi:10.1002/jgrf.20146.
- Zwally, H. J., W. Abdalati, T. Herring, K. Larson, J. Saba, and K. Steffen (2002), Surface melt-induced acceleration of Greenland ice-sheet flow, *Science*, 297(5579), 218–222, doi:10.1126/science.1072708.